Laboratory scale production of complex protein substrates using substrate-complimentary nanoenvironments

Siddharth Deshpande
Yong Loo Lin School of Medicine, National University of Singapore
Samira Sadeghi
Yong Loo Lin School of Medicine, National University of Singapore
Girish Mavelli Vallerinteavide
Yong Loo Lin School of Medicine, National University of Singapore
M. Alphan Aksoyoglu
Jacobs University https://orcid.org/0000-0002-8301-8315
Jayesh Bafna
Jacobs University
mathias winterhalter
Jacobs University Bremen https://orcid.org/0000-0002-1604-3318
Manjunatha Kini
National University of Singapore
David Lane
Agency for Science, Technology and Research https://orcid.org/0000-0003-0551-3545
Chester Drum (mdccld@nus.edu.sg)
National University of Singapore

Article

Keywords: Protein nanoparticle, Thermostable ExoShell, Protein refolding, P53

Posted Date: May 13th, 2021

DOI: https://doi.org/10.21203/rs.3.rs-469958/v1

Version of Record: A version of this preprint was published at Nature Communications on September 29th, 2021. See the published version at https://doi.org/10.1038/s41467-021-25996-4.

Abstract

In vitro protein folding is a complex process which often results in protein aggregation, low yields and low specific activity. We report the use of nanoscale exoshells (tES) to provide specific nanoenvironments for the folding and release of 12 highly diverse protein substrates ranging from small protein toxins to human albumin, a dimeric protein (alkaline phosphatase), a trimeric ion channel (Omp2a) and the tetrameric tumor suppressor, p53. These proteins represent a unique diversity in size, volume, disulfide linkages, isoelectric point and multi versus monomeric nature of their functional units. Crude soluble yield (3-fold to > 100-fold), functional yield (2-fold to > 100-fold) and specific activity (3-fold to > 100-fold) were increased for all the proteins tested. The average soluble yield of POI was 6.5 mg/100 mg of tES. Charge complementation between the tES internal cavity and the protein substrate was the primary determinant in functional folding. Our results confirm the importance of nanoscale electrostatic effects and provide a novel nanoparticle solution for folding proteins in vitro.

Introduction

Efficient folding of proteins in vitro has been a goal of biochemistry since the early experiments of Anfinsen[1]. In practice, the pathway from a linear polypeptide to a functional macromolecule remains complex and often ends in an insoluble or improperly folded product[2]. Natural chaperone proteins operate on a nanoscale. These endogenous nanoparticles help to reduce aggregation and structural heterogeneity through the use of long-range electrostatic interactions, short-range hydrophobic forces and the physical confinement of protein substrates within a chaperone cage[3]. The use of chaperones for in vitro protein production, however, is rare as they are difficult to produce at scale, have limited effect sizes and are are characterized for only a single, or very few, protein substrates [4, 5]. In a compendium of 1,046 in vitro folding protocols (RefoldDB), only 6 protocols (0.5%) incorporate an added chaperone for protein folding[6].

We have previously shown that macromolecules covalently fused to the interior of a protein nanoshell can fold and be protected from external denaturants, however produce low yields[7]. We thus test the hypothesis that thermostable exoshells (tES) can non-covalently encapsulate, fold, promote disulfide pairing and release proteins of interest (POI) with full protein function and at suitable scale (milligrams / litre culture) for laboratory use (Fig. 1a; Figure S1). Compared to the use of fusion proteins, diffusion-based loading offers (i) far greater yields of POI (~ 5 mg / 100mg of tES versus < 5 ug / 100 mg of tES for the fusion protein approach), (ii) improved quality of folded product (i.e., specific activity) compared with non-tES mediated folding and (iii) a protocol simple enough to be used by non-biochemistry labs.

Experimental Section

Comparisons of tES nanoparticlefolding

tES shells are 24-mers of a single truncation of the native sequence from *Archeoglobus fulgides*. Monomers contain histidine substitutions at sites of 3-fold symmetry (F116H) to resulte in pH titratable assembly and disassembly of the shell. To provide charge complementation of client proteins, tES(F116H) variants have net positive [tES-F116H(+)], negative [tES-F116H(-)] and neutral [tES-F116H(+/-)] interior charges. All three variants of tES can be expressed (≥ 400 mg L^{-1} shaking flask cell culture), purified (≥ 90%) and concentrated (200mg mL^{-1}) using standard techniques.

Twelve proteins (Figure S2) were individually expressed as denatured inclusion bodies to serve as a panel to characterize the effect of tES. Briefly, purified tES-F116H shells were mildly acidified for disassembly (pH < 6.0), following which the subunits were separated in size-exclusion chromatography (SEC). POI samples in solubilization buffers were incubated in the presence of tES subunits at different ratios until the optimum POI - tES ratio was reached for maximum encapsulation efficiency. The pH of the mixture was adjusted to 8.0 followed by overnight dialysis in refolding buffer (Figure S1). The refolded protein was purified using SEC and checked for its activity.

Crude soluble yield for POIs was increased upon tES-F116H encapsulation. Except for 3 proteins that showed moderate increase, crude soluble yield for the majority of tES-F116H:POI demonstrated much higher values (Figure 1b,c). Maximum tES-F116H:POI encapsulation ratios were measured for proteins rFasxiator, rLuc, HSA, sAP, Omp2a and p53 (Figure S3). Observed ratios were found to be in strict accordance with the calculated POI molecular volumes and the steric upper limit of the tES-F116H shell interior (tES-F116H shell interior ($3.2x10^5$ Ang^3)[8]. Of note, we attempted to study encapsulation of two conotoxins (1.2-1.4 kDa), however, the M.W. of tES-F116H:POI dynamically decreased throughout the analytical ultracentrifugation (AUC) run (Figure S3). We hypothesize that the conotoxins are initially encapsulated but escape through the 4 nm triangular pores of tES during sedimentation.

Optimal ratios of tES:POI for functional yield were determined for 9 monomeric POIs. POIs were titrated against a fixed concentration of tES and after removal of denaturant and protein aggregates, when possible the soluble fraction was quantified using individual activity assays generally performed while the monomer was still inside the shell (conotoxin and rFasxiator assays required release from the shell). The relationship of tES:POI functional yield demonstrated a sigmoidal distribution for all POI (Figure 1d; Figure S2). The saturation point for tES:POI functional yield generally followed the predicted steric limits of encapsulation, i.e., for tES:conotoxins (60:150), tES:rFasxiator/PLA2 (60:15), tES:HRPc/GFPuv/rLuc (60:10) and tES:FFL/HSA (60:5) (Figure S4-S6). The pattern of functional yields closely paralleled the titrated thermal stabilities seen with Differential Scanning Fluorimetry (DSF), suggesting that thermodynamic stabilization of the tES-F116H:POI complex may facilitate substrate folding. Of note, the two small (~1 kDa) conotoxins required much higher ratios to stabilize the tES nanoparticle. In addition, we measured the zeta potential of the 9 monomeric POIs (Figure S6d). For both functional yield and thermodynamic stabilization, tES-F116H to POI charge pairing determined the optimal approach for all cases. In particular, charge mismatch samples showed no difference in stabilization compared with tES alone (Figure 1e). Each of three tES charge variants was then tested under saturating conditions as determined in Figure 1f. A consistent association between POI charge, tES internal charge and tES

denaturation temperature can be seen (Figure 1e) for all substrates, with opposite charge pairing providing thermal stabilization and same-charge pairing resulting in tES denaturation temperatures no different than tES alone (Figure 1e,f). All 12 tES:POI complexes demonstrated monodisperse, 12nm radii in solution (Figure S7) and the expected spherical morphology on transmission electron microscopy (Figure S8) suggesting the encapsulation process did not affect the final tES assembly. In addition, all three tES-F116H charge variants show stability of secondary structure to ~90°C, and can undergo at least 10 rounds of pH titrated (pH 5.8 - pH 8.0) assembly and disassembly without precipitation or significant protein loss (Figure 1g).

Protein-specific applications of engineered nanoenvironments (monomers)

Small protein toxins

The diverse effects of small peptide toxins have contributed to fundamental advances in neuroscience, in addition to the design of approved therapeutics[9]. Aggregation and structural heterogeneity often prevent the folding of synthetic peptide toxins in vitro[10, 11]. The effect of tES was tested with three structurally distinct toxins. α-conotoxin (lml P6 amide, 1.35 kDa) is a 12 amino acid peptide with a net positive surface charge. α-conotoxin can form either a bio-active conformation (C1-3/C2-4) or bio-inactive conformations depending on the disulfide pairing of four cysteine residues (C1-4/C2-3 or C1-2/C3-4). λ-conotoxin (CMrVIA K6, 1.24 kDa) has 10 amino acids, a net neutral charge and likewise can fold into bio-active (C1-4/C2-3) or bio-inactive (C1-3/C2-4 and C1-2/C3-4) conformations based on the disulfide pairing of four cysteines[11]. When the tES charge complemented the net charge of the peptide, i.e., tES-F116H(-) for α-conotoxin and tES-F116H(+/-) for λ-conotoxin, tES increased crude soluble yield (60-fold for both) functional yield (10-fold for both) and specific activity (8-fold for α-conotoxin and 4-fold for λ-conotoxin) (Figure 1b-d; Figure 2a,b,j and k; Figures S9, S10).

rFasxiator (12 kDa) is a Kunitz-type inhibitor of factor XIa, has a net positive charge and three disulfide bridges[12]. The use of tES-F116H(-) with rFasxiator increased crude soluble yield (3-fold), functional yield (3-fold), and specific activity (4-fold) (Figure 1b-d; Figure 2c,l; Figure S11a; Figure S12c). We measured biochemical encapsulation ratios using analytical ultracentrifugation (AUC). Three rFasxiator molecules were encapsulated per tES-F116H(-) whereas the same charge tES-H116(+) showed no encapsulation (Figure 3a,b).

Phospholipase A_2

Acidic phospholipase A_2 (PLA_2, 17 kDa) is a calcium-dependent enzyme found in snake venom (*Agkistrodon halyspallas*) which cleaves fatty acids from phospholipids resulting in arachidonic acid release and localized inflammation[13]. PLA_2 is negatively charged, contains seven conserved disulfide bridges and no prior in vitro folding studies have been reported and extensive precipitation was noted in the POI-only refolding mix. tES-F116H(+) increased crude soluble yield (500-fold), functional yield (13-fold) and specific activity (20-fold) of PLA_2 (Figure 1b-d; Figure 2d,m; Figure S11b).

Green fluorescent protein

Green fluorescent protein (GFPuv, 27 kDa) is a negatively charged model protein for folding studies and undergoes highly variable expression in *E.coli*, dependent on induction conditions[14]. Correct folding of the native GFPuv structure can be inferred from the development of 508 nm fluorescence which requires autocatalytic formation of the fluorophore and a surrounding β-barrel structure. GFPuv overexpression in *E. coli* results in both soluble and insoluble fractions. tES-F116H(+) folding of GFPuv inclusion bodies increased crude soluble yield (900-fold), functional yield (30-fold) and specific activity (30-fold). GFPuv purified from the soluble fraction of *E. coli* (h6s) exhibited comparable specific activity (0.8-fold) to tES-F116H(+) folded GFPuv (Figure 1b-d; Figure 2e,n; Figure S11c).

Horseradish peroxidase

Horseradish peroxidase (HRP) is an industrial enzyme used in chromogenic assays however requires production from the root of the horseradish plant (*Armoracia rusticana*) resulting in seasonal yields and a heterogenous mixture of isoenzymes[15]. We studied recombinant expression of HRP isozyme C (HRPc, 34 kDa), a truncated version of HRP, which forms inactive inclusion bodies in *E. coli*. Refolding of HRPc requires the presence of calcium, formation of four disulfide bonds, the incorporation of a heme prosthetic group and currently results in low yields (2-3%) of active enzyme[16]. tES-F116H(+) increased crude soluble yield (1,400-fold), functional yield (18-fold) and specific activity (2-fold) of HRPc (Figure 1b-d; Figure 2f,o; Figure S11d).

Renilla luciferase

Renilla luciferin 2-monooxygenase (rLuc, 36 kDa) is a negatively charged, easily denatured intracellular protein which catalyzes coelenterazine substrate in the presence of oxygen to produce blue light[17]. Factors which effect the folding of rLuc are unknown as in vitro folding of rLuc has not been previously reported. tES-F116H(+) increased crude soluble yield (3-fold), functional yield (21-fold) and specific activity (30-fold) (Figure 1b-d; Figure 2g,p; Figure S11e; Figure S12b). Using AUC, we found a ratio of two rLuc molecules to each tES-F116H(+). tES-F116H(+) demonstrated maximal encapsulation compared to tES-F116H(+/-) and tES-F116H(-); with a consistent peak broadening corresponding to an additional population of tES with a single rLuc (Figure 3c,d)

Firefly luciferase

Firefly luciferase (FFL, 60 kDa) is a negatively charged bioluminescent protein widely used in bioassays that oxidizes luciferin substrate in the presence of ATP, Mg^{2+} ion and oxygen. FFL serves as a model for the study of ATPase enzymes; however, folding and stability of FFL remains a significant challenge[18]. The structural fold of FFL is not related to rLuc and consists of two lobular domains that exist in either an extended conformation (which would exceed the internal diameter of the tES cage) or a compact conformation with substrate bound at the domain interface[17]. tES-F116H(+/-) increased crude soluble

yield (10-fold), functional yield (8-fold) and specific activity (7-fold) of FFL (Figure 1b-d; Figure 2h,q; Figure S11f).

Human albumin

Human serum albumin (HSA, 66 kDa) is the most abundant protein in blood and is an important infusional therapeutic. Recombinant expression and in vitro folding protocols for HSA have proven difficult and HSA currently requires purification from human blood products[19]. HSA is a globular protein with three α-helical domains and seventeen disulfide bonds and which complicates in vitro folding due to the formation of inappropriate inter-domain pairing[20]. tES-F116(+) increased crude soluble yield (1,800-fold), functional yield (4-fold) and specific activity (5-fold) of HSA (Figure 1b-d; Figure 2i,r; Figure S11g; Figure S12a). Using AUC, we found a ratio of a single HSA molecule to each tES-F116H(+) whereas tES-F116H(+/-) and tES-F116H(-) encapsulate either not at all or with very low frequency (Figure 3e,f).

Protein-specific applications of engineered nanoenvironments (multimers)

30-50% of all proteins exist natively as homo-multimers, yet only few solutions exist for in vitro folding of multimeric proteins[21]. The natural assembly of protein multimers is thought to occur sequentially. A polypeptide first folds into a "structured monomer", which then associates with other subunits to form, after further conformational changes, a multimeric assembly. Structured monomers are inherently unstable and often rely on chaperones to produce the appropriate fold required for quaternary assembly[22]. We hypothesized that structural monomers could be folded, transiently stabilized and, upon release from tES-F116H nanoparticle, mutually assemble without aggregation in vitro.

Alkaline phosphatase, a dimeric enzyme

Alkaline phosphatases (AP) are negatively charged homo-dimeric metalloenzymes which contain two intrachain disulfide bonds and are used widely in both industry and research[23]. An exception to this is a monomeric form of AP isolated from the Vibrio genus[24]. Shrimp AP (sAP, 52 kDa) is active at low temperatures (0-15 °C) and denatures above 30 °C, resulting in its extensive use for cloning protocols[25]. The thermolability of sAP makes it a challenge for in vitro folding and no in vitro folding protocols have been published. APs have been reported to form numerous intermediate proteins during both unfolding and refolding processes[26] and when sAP is folded in vitro without tES, it aggregates and fails to form dimers (Figure 4a). Consistent with a hypothesis of structured monomer assembly, the use of charge-complementary tES to fold sAP was critical for sAP dimer formation (Figure 4a). The role of zinc and magnesium ions in sAP function and folding were likewise studied and consistent with prior reports[27]. tES-F116H(+) crude soluble yield (60-fold), increased functional yield (9-fold) and specific activity (10-fold) of sAP (Figure 1b,c; Figure 4b-e) No dimer formation was observed when sAP was folded in the absence of tES (Figure 4a).

Because the steric limit of tES enforces monomeric encapsulation, isolated subunits of multimeric enzymes can be studied in solution. The active site of AP does not require catalytic residues contributed from a paired dimer and, interestingly, thermolabile, monomeric isoforms of AP can be isolated from cold-adapted Vibrio species[28]. After confirming monomeric encapsulation via AUC (Figure 4f) and isolating tES-F116H:sAP complexes, we found remarkable activity of the sAP monomer while it was encapsulated in the tES-F116H(+) cage and only a 2-fold activity increase after release from tES (Figure 4g,h). This stands in contrast to a study of *E. coli* AP which reported a 10,000-fold difference in monomeric versus dimeric activity[29]. Consistent with our findings, Olsen et al. have reported sAP to be a homo-dimer in solution, however, observed in situ catalytic activity for sAP monomers separated via native gel electrophoresis[30]. The specific activity of sAP dimer released from tES was equivalent to a positive control whereas activity of encapsulated sAP monomers was reduced by ~50% (Figure 4b,c).

Omp2A, a trimeric ion channel

Porins are homo-trimeric ion channels natively expressed in the outer membrane of bacteria, mitochondria and chloroplasts. Omp2a (39 kDa) is a negatively charged porin isolated from *Brucella melitensis*, studied for its biophysical properties and as an antigen for the prevention of brucellosis. Omp2a is toxic when overexpressed as a soluble protein and is thus purified as an inclusion body[31]. Production of Omp2a, and porins in general, thus remains a significant challenge for studies of channel function. We performed nanoencapsulation using three tES charge variants on Omp2a and, using AUC, found a shift in M.W (Figure 5a). consistent with a single encapsulated monomer per either tES-F116H(+) or tES-F116H(+/-) shell. No encapsulation was seen with tES-F116H(-) (Figure 5a). Following the nanoencapsulation protocol and substrate release, Omp2a subunits were subjected to a 9-day incubation period at 37 °C (Figure 5b). Size profiles were assessed via sequential sampling and SEC analysis (Figure 5c-e). AUC confirmed that only Omp2a subunits released from tES-F116H(+) formed a monodisperse peak at 170 kDa, consistent with complete trimerization (Figure 5f). When Omp2a was folded within tES-F116H(+/-) it partially multimerized into trimers after 9 days, however when Omp2a was folded under identical conditions without tES, or using tES-F116H(-), no evidence of trimer assembly was seen on SEC or AUC. (Figure 5a,f).

Tryptophan fluorescence is a measure of Omp2a folding[31] and was increased following Omp2a trimerization (Figure 5g). To confirm ion channel activity of the assembled trimers, the tES-F116H(+) folded Omp2a 170 kDa fraction was studied in membrane bilayers. In a prior study, Omp2a protein was found to be unstable, conductances were highly variable (~45 pS-650 pS) and no trimer activity could be observed[32]. In our study, Omp2a trimers demonstrated conductances of 3 nS or 4 nS with occasional conductances of 1 nS (Figure 5h). As no electrophysiological characterizations of Omp2a trimer formations have been reported for comparison, we used the method of Roussel et al to obtain small amounts of Omp2a trimers[33] and no differences in conductance or gating were observed (Figure 5i). The gating and conductance of trimeric Omp2a thus appears to be similar to its trimeric homologue,

Omp2b[32]. tES-F116H(+) increased crude soluble yield (900-fold), functional yield (>100-fold) and specific activity (>100-fold) of Omp2 (Figure 1b,c; Figure 5h).

p53, a tetrameric tumor suppressor

Tumor protein 53 (p53, 43.7 kDa) is a homo-tetrameric tumor suppressor and the most commonly mutated gene (>50%) in human cancers[34]. Tetramerization of p53 monomers is essential for biological activity and hetero-multimerization with p53 mutants can account for the differential penetrance of common cancer mutations[35]. Post-translational modifications of p53 are complex and regulate multiple cellular functions including coordination of apoptosis, senescence and response to physiological stress[36]. The production of stable, unmodified p53 monomers which are able to form functional tetramers in vitro is thus critical for the bio study of p53 as a regulatory node in cellular signaling.

E. coli express recombinant p53 as an insoluble inclusion body and in vitro folding typically results in low yields[37]. We tested the hypothesis that encapsulation of p53 monomers in tES would promote structure formation without aggregation and result in spontaneous tetramer formation upon release from the shell. A single monomer was encapsulated within tES-F116H(+) and tES-F116H(+/-), however, no encapsulation was observed with tES-F116H(-) (Figure 6a). After protein release, a 174 kDa SEC peak was observed consistent with tetrameric p53 with the largest yield resulting from use of tES-F116H(+/-) (Figure 6b). Prior to tES release, p53 was visualized using SDS PAGE as a 47 kDa monomer. After tES release, p53 was predominantly seen as a ~180 kDa band which was attributed to the tetramer. Upon denaturation (boiling) of the same sample, the tetramer band disappeared and a 47 kDa monomer band was visible (Figure 6c).

We found that p53 folded using tES-F116H(+/-) exhibits a clear dF/dt peak at a slightly higher denaturation temperature of 50 °C (Figure 6d). Whereas PAb1620 antibody alone resulted in a negative dF/dt deflection at 78 °C, when PAb1620 was combined with p53, the 50 °C p53 denaturation peak disappeared, the PAb1620 negative deflection was reduced and a new dF/dt peak at ~ 94 °C appeared, which was attributed to the p53:PAb1620 complex (Figure 6d). A similar, but lesser, effect was seen with tES-F116H(+) folded p53 (Figure 6e), however mixing PAb1620 with p53 folded without tES or p53 folded with tES-F116H(-) did not exhibit evidence of p53 stabilization or a PAb1620:p53 complex (Figure 6f,g). Similar to PAb1620, PAb240 also exhibited a downward deflection of dF/dt at 78 °C. When mixed with tES-F116H(+/-) folded p53, no evidence of complexation was seen. When PAb240 was mixed with p53 folded alone and with p53 folded using tES-F116H(-), a new denaturation peak (almost identical to the PAb1620:p53 complex peak) was observed at 94 °C, which was attributed to the PAb240:p53 complex (Figure 6h-k)

P53 is a transcription factor and to test the function of tES-F116H - folded p53, we measured sequence specific binding to consensus p53 response element (conA), a 20 b.p. DNA oligomer which binds tetrameric p53[38]. Similar to our observations with antibody stabilization, mixing conA with folded p53 ablated the 49 °C p53 denaturation peak in DSF in addition to a reduction of the DNA denaturation peak

at 27 °C. Likewise, a new negative deflection peak centered around 55 °C was attributed to the conA:p53 complex. A scrambled version of conA showed no effect on p53 stabilization or complex formation (Figure 6l). AUC analysis of tES-F116H(+/-) folded p53 and conA further showed a 360 kDa complex consistent with a stable conA:p53 complex whereas scrambled conA showed no evidence of complex formation (Figure 6l,m). Overall, tES-F116H(+/-) provided optimal folding of p53. Although tES-F116H(+) also demonstrated positive effects on folding, tES-F116H(-) failed to produce p53 tetramers. tES-F116H(+/-) increased p53 crude soluble yield (950-fold), functional yield (10.5-fold) and specific activity (12-fold) (Figure 1b,c; Figure 6n,o).

Discussion

Nanoencapsulation within the 8nm aqueous cavity of tES-F116H appears to exert a broad effect across protein classes and is governed by basic biophysical principles. tES recapitulates a mechanism used by the evolutionarily conserved GroEL/ES chaperonin, which folds peptides in a similar size 8 nm x 8 nm cylindrical cavity. Thermodynamic models suggest that the 8nm scale of the GroEL/ES cavity plays a major role in the stabilization of proteins and studies which empirically vary the volume of GroEL/ES demonstrate large effects on substrate folding[39]. This data suggests that the scale of the tES-F116H interior, itself, may play a significant role in our observed results. On the basis of the measured cis cavity volume of 175,000A^3 and the assumption that partial specific volume of a folded POI is 1.23A^3 Da^{-1}, GroEL/ES systems can accommodate up to ~140kDa proteins[40]. Similar to this, we assume that tES can encapsulate spherical POIs up to ~260kDa within the calculated volume of 324,900A^3[8]. Because ~80% of translated monomeric proteins are less than 80 kDa , the majority of expressed monomers in nature would be potential candidates for tES.

GroEL/ES is different from tES in that it uses ATP binding to alternate exposure of hydrophobic and hydrophilic residues and ATP hydrolysis to propagate a reaction cycle of iterative protein annealing[41]. Although tES nanoparticle does not undergo allosteric changes, the addition and removal of chaotropes while the POI remains confined inside the tES shell may approximate a single annealing step of GroEL/ES, albeit orders of magnitude slower. Similar in theme to tES-F116H are GroEL/ES variants, namely SR1/GroES, which lack ATPase ability yet retain protein folding efficiency[42].

Currently, there are no platform solutions for protein folding in vitro. Although we report the largest sampling of protein size, molecular volume, conformation, isoelectric point, percentage of secondary structure, cysteine density and monomeric versus multimeric functional units to date; there are, nonetheless, biases incorporated into our test set (Figure S2). Primarily, we focused on proteins which have a tractable activity assay, thus classes of proteins such as scaffolding and binding modulators are not included. Secondly, our sample set is biased to proteins with monomeric molecular weight below 80kDa. Thirdly, although all proteins are expressed and purified as denatured inclusion bodies, one of the proteins we attempted to study (trypsin) was unexpressable in E.coli, presumably due to intracellular

toxicity. Thus, an additional important bias is that all studied proteins were biologically compatible with the expression host.

Overall, tES nanoparticles address critical gaps in the field of in vitro folding as they can be easily purified in large amounts, stored at room temperature and exhibits structural stability in the strong denaturants required of denatured protein solubilization[7]. tES may be helpful in additional applications that require a charge complementary environment and avoidance of aggregation[43]. Although this study advances tES bioproduction beyond a proof of concept to laboratory scale production, further investigation will be required for industrial scale production of biologicals using tES.

Declarations

Conflict of Interest:

The authors declare that they have no conflict of interest.

References

[1] C. B. Anfinsen, Science 1973, 181, 223.

[2] N. Kannan, S. Vishveshwara, Journal of molecular biology 1999, 292, 441.

[3] P. Koldewey, F. Stull, S. Horowitz, R. Martin, J. C. Bardwell, Cell 2016, 166, 369; H. Saibil, Nature reviews Molecular cell biology 2013, 14, 630.

[4] F. U. Hartl, M. Hayer-Hartl, Nature structural & molecular biology 2009, 16, 574.

[5] K. Jhamb, A. Jawed, D. K. Sahoo, Process Biochemistry 2008, 43, 587.

[6] H. Mizutani, H. Sugawara, A. M. Buckle, T. Sangawa, K.-i. Miyazono, J. Ohtsuka, K. Nagata, T. Shojima, S. Nosaki, Y. Xu, BMC structural biology 2018, 17, 1.

[7] S. Deshpande, N. D. Masurkar, V. M. Girish, M. Desai, G. Chakraborty, J. M. Chan, C. L. Drum, Nature communications 2017, 8, 1.

[8] E. Johnson, D. Cascio, M. R. Sawaya, M. Gingery, I. Schröder, Structure 2005, 13, 637.

[9] M. W. Pennington, A. Czerwinski, R. S. Norton, Bioorganic & medicinal chemistry 2018, 26, 2738.

[10] A.-H. Jin, M. Muttenthaler, S. Dutertre, S. Himaya, Q. Kaas, D. J. Craik, R. J. Lewis, P. F. Alewood, Chemical reviews 2019, 119, 11510.

[11] G. Bulaj, B. M. Olivera, Antioxidants & redox signaling 2008, 10, 141.

[12] W. Chen, L. Carvalho, M. Chan, R. Kini, T. Kang, Journal of Thrombosis and Haemostasis 2015, 13, 248.

[13] X. Liu, H. Pan, G. Yang, X. Wu, Y. Zhou, Biochimica et Biophysica Acta (BBA)-Protein Structure and Molecular Enzymology 1999, 1431, 157.

[14] G. S. Waldo, B. M. Standish, J. Berendzen, T. C. Terwilliger, Nature biotechnology 1999, 17, 691; H. Fukuda, M. Arai, K. Kuwajima, Biochemistry 2000, 39, 12025.

[15] N. C. Veitch, Phytochemistry 2004, 65, 249.

[16] S. Asad, B. Dabirmanesh, N. Ghaemi, S. M. Etezad, K. Khajeh, Molecular biotechnology 2013, 54, 484.

[17] N. Thorne, J. Inglese, D. S. Auld, Chemistry & biology 2010, 17, 646.

[18] M. S. Svetlov, A. Kommer, V. A. Kolb, A. S. Spirin, Protein science 2006, 15, 242.

[19] A. Sharma, T. K. Chaudhuri, Microbial cell factories 2017, 16, 1.

[20] S. J. BURTON, A. V. QUIRK, P. C. WOOD, European journal of biochemistry 1989, 179, 379.

[21] E. D. Levy, S. A. Teichmann, Progress in molecular biology and translational science 2013, 117, 25.

[22] B. J. Pieters, M. B. Van Eldijk, R. J. Nolte, J. Mecinović, Chemical Society Reviews 2016, 45, 24.

[23] J. E. Coleman, Annual review of biophysics and biomolecular structure 1992, 21, 441.

[24] N. K. Roy, R. K. Ghosh, J. Das, Journal of bacteriology 1982, 150, 1033.

[25] M. de Backer, S. McSweeney, H. B. Rasmussen, B. W. Riise, P. Lindley, E. Hough, Journal of molecular biology 2002, 318, 1265.

[26] H.-C. Hung, G.-G. Chang, Biophysical Journal 2001, 81, 3456.

[27] Y. Akiyama, K. Ito, Journal of Biological Chemistry 1993, 268, 8146; Y.-X. Zhang, Y. Zhu, H.-W. Xi, Y.-L. Liu, H.-M. Zhou, The international journal of biochemistry & cell biology 2002, 34, 1241.

[28] J. B. Hauksson, Ó. S. Andrésson, B. Ásgeirsson, Enzyme and microbial technology 2000, 27, 66.

[29] R. R. Boulanger Jr, E. R. Kantrowitz, Journal of Biological Chemistry 2003, 278, 23497.

[30] R. L. Olsen, K. Øverbø, B. Myrnes, Comparative Biochemistry and Physiology Part B: Comparative Biochemistry 1991, 99, 755.

[31] G. Roussel, A. Matagne, X. De Bolle, E. Perpète, C. Michaux, Protein expression and purification 2012, 83, 198.

[32] H. Mobasheri, T. Ficht, H. Marquis, E. Lea, J. Lakey, FEMS microbiology letters 1997, 155, 23.

[33] M. Bannwarth, G. E. Schulz, Biochimica et Biophysica Acta (BBA)-Biomembranes 2003, 1610, 37; G. Roussel, E. A. Perpète, A. Matagne, E. Tinti, C. Michaux, Biotechnology and bioengineering 2013, 110, 417.

[34] E. R. Kastenhuber, S. W. Lowe, Cell 2017, 170, 1062.

[35] W. M. Chan, W. Y. Siu, A. Lau, R. Y. Poon, Molecular and cellular biology 2004, 24, 3536.

[36] A. M. Bode, Z. Dong, Nature Reviews Cancer 2004, 4, 793.

[37] M. LaFevre-Bernt, S. Wu, X. Lin, Molecular cancer therapeutics 2008, 7, 1420.

[38] W. S. El-Deiry, S. E. Kern, J. A. Pietenpol, K. W. Kinzler, B. Vogelstein, Nature genetics 1992, 1, 45.

[39] F. Takagi, N. Koga, S. Takada, Proceedings of the National Academy of Sciences 2003, 100, 11367; A. Brinker, G. Pfeifer, M. J. Kerner, D. J. Naylor, F. U. Hartl, M. Hayer-Hartl, Cell 2001, 107, 223.

[40] Z. Xu, A. L. Horwich, P. B. Sigler, Nature 1997, 388, 741.

[41] D. K. Clare, D. Vasishtan, S. Stagg, J. Quispe, G. W. Farr, M. Topf, A. L. Horwich, H. R. Saibil, Cell 2012, 149, 113.

[42] J. S. Weissman, H. S. Rye, W. A. Fenton, J. M. Beechem, A. L. Horwich, Cell 1996, 84, 481; M. Mayhew, A. C. da Silva, J. Martin, H. Erdjument-Bromage, P. Tempst, F. U. Hartl, Nature 1996, 379, 420.

[43] R. J. Ellis, Current Biology 2003, 13, R881; R. J. Ellis, Nature 2006, 442, 360.

Figures

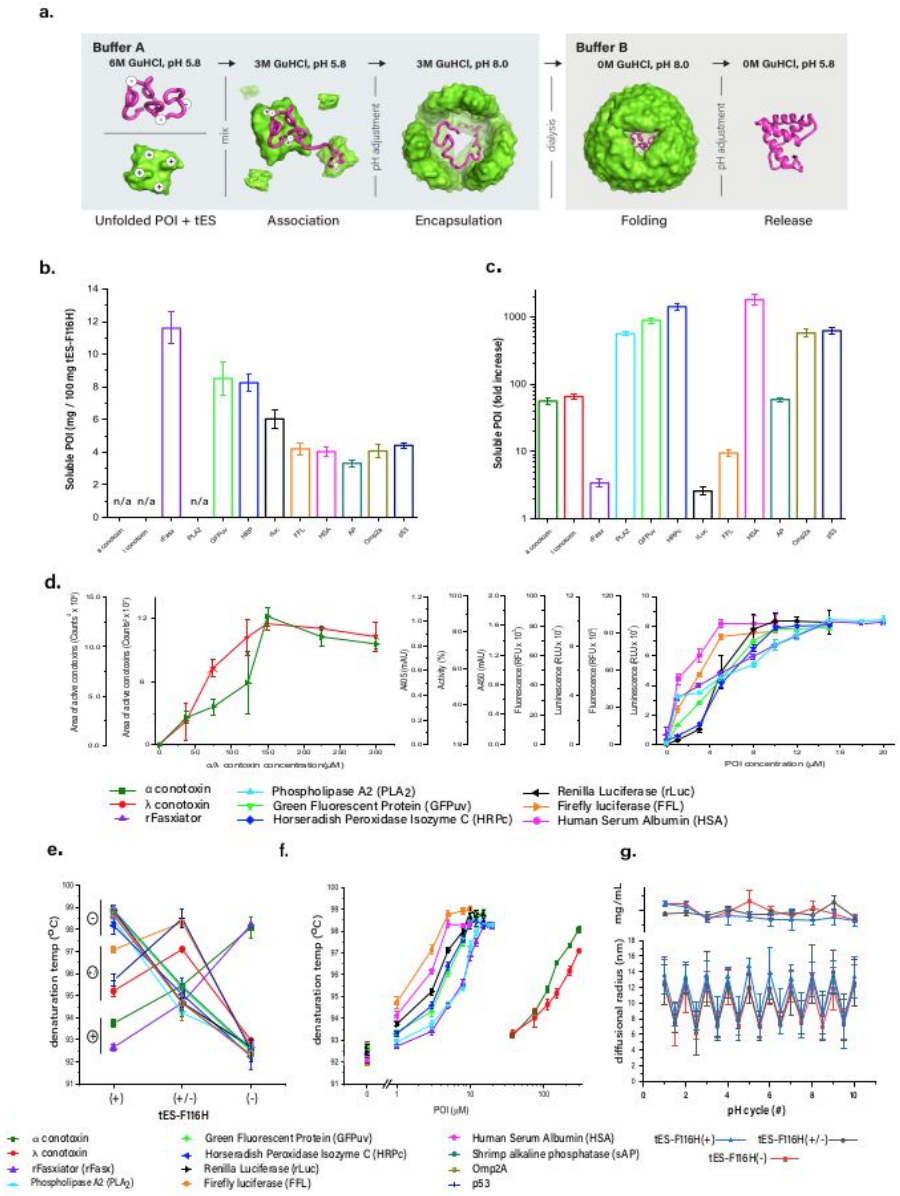

Fig. 1 | Comparisons of tES-F116H folding . a, Description of the tES nanoencapsulation protocol depicting buffer adjustments and buffer exchange via dialysis **b**, Crude soluble yields of POI increase after tES-F116H nanoencapsulation. As the amount of tES added to the folding mix was the limiting factor for POI soluble yield, results are expressed as mg POI / 100 mg tES-F116H. **c**, Fold-increase comparisions of soluble POI folded with and without tES-F116H. **d**, Functional yields of POI are determined by the ratio of POI to tES-F116H in the folding mix and demonstrate saturation with titration. **e**, Charge complementation of the tES-F116H interior with POI determines stabilizing energetics. Three tES-F116H charge variants are assayed and POI self organize according to their charge (labelled next to the ordinate) and stabilizing effect. **f**, Low molecular weight proteins require high molar ratios to stabilize the assembly. Thermal denaturation temperatures of tES-F116H were measured via DFS as the concentation of POI is titrated against tES-F116H during the loading phase of the folding protocol. **g**, tES-F116H undergo pH mediated assembly and disassembly. Shell diameter can be monitored using DLS (lower panel) and no significant soluble protein loss is observed after 10 cycles (upper panel). Titration of POI results in shifts of tES-F116H mass consistent with the steric limits of the tES interior (~80 kDa).

Figure 1

Comparisons of tES-F116H folding . a, Description of the tES nanoencapsulation protocol depicting buffer adjustments and buffer exchange via dialysis b, Crude soluble yields of POI increase after tES-F116H nanoencapsulation. As the amount of tES added to the folding mix was the limiting factor for POI soluble yield, results are expressed as mg POI / 100 mg tES-F116H. c, Fold-increase comparisions of soluble POI folded with and without tES-F116H. d, Functional yields of POI are determined by the ratio of

POI to tES-F116H in the folding mix and demonstrate saturation with titration.c, Charge complementation of the tES-F116H interior with POI determines stabilizing energetics. Three tES-F116H charge variants are assayed and POI self organize according to their charge (labelled next to the ordinate) and stabilizing effect. f, Low molecular weight proteins require high molar ratios to stabilize the assembly. Thermal denaturation temperatures of tES-F116H were measured via DFS as the concentation of POI is titrated against tES-F116H during the loading phase of the folding protocol. g, tES-F116H undergo pH mediated assembly and disassembly. Shell diameter can be monitored using DLS (lower panel) and no significant soluble protein loss is observed after 10 cycles (upper panel). Titration of POI results in shifts of tES-F116H mass consistent with the steric limits of the tES interior (~80 kDa).

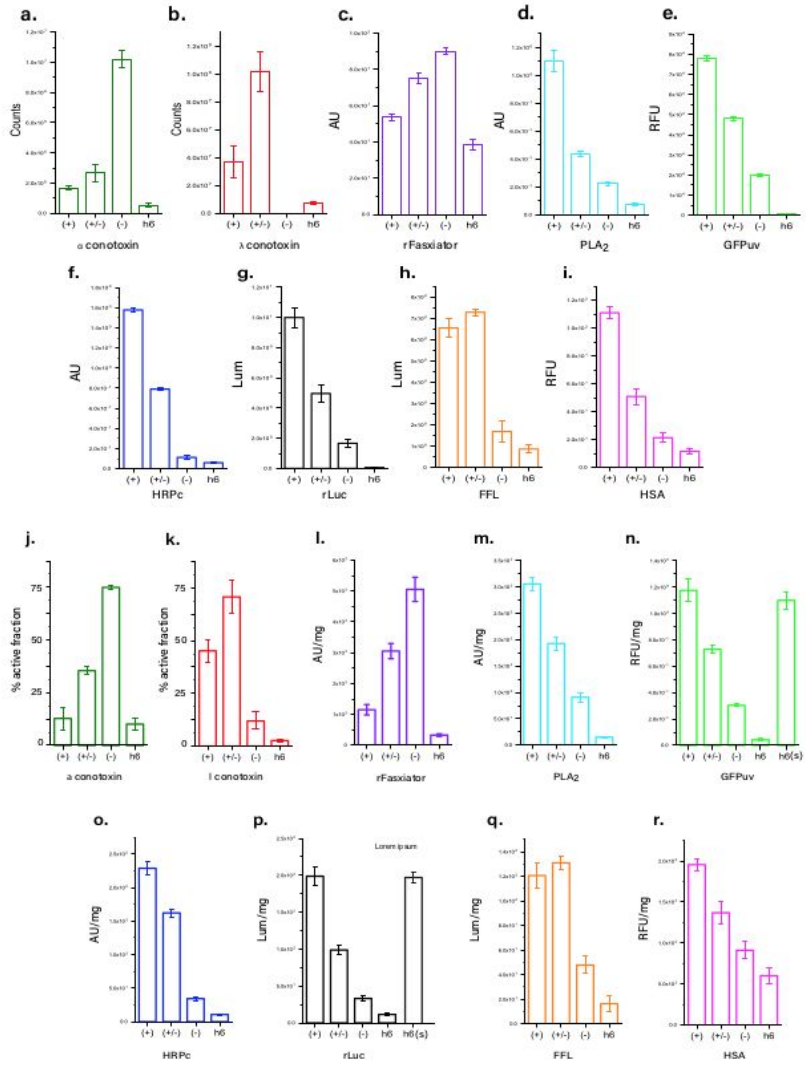

Fig. 2 | Effect of tES-F116H on POI activity. a-i, Activity assays of POI after folding with tES-F116H charge variants and in the abscence of tES-F116H. **j-r,** Specific actity is increased after tES-F116H folding when compared with the respective POI-only folding control. tES-F116H(+), tES-F116H(+/-), tES-F116H(-) and POI-alone are indicated as (+), (+/-), (-) and h6, respectively. GFPuv and rLuc, also expressed as a soluble protein, thus POI purified from this soluble fraction is indicated as h6(s) and used as positive control.

Figure 2

Effect of tES-F116H on POI activity. a-i, Activity assays of POI after folding with tES-F116H charge variants and in the abscence of tES-F116H. j-r, Specific actity is increased after tES-F116H folding when compared with the respective POI-only folding control. tES-F116H(+), tES-F116H(+/-), tES-F116H(-) and POI-alone are indicated as (+), (+/-), (-) and h6, respectively. GFPuv and rLuc, also expressed as a soluble protein, thus POI purified from this soluble fraction is indicated as h6(s) and used as positive control.

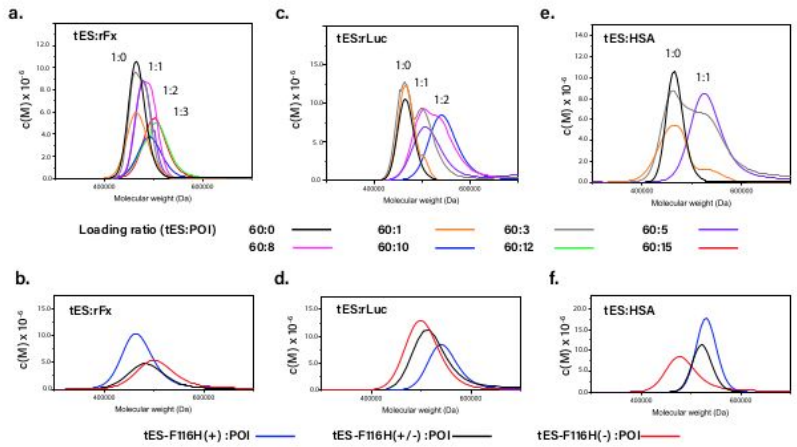

Fig. 3 | Monomeric POI encapsulation using tES-F116H a, tES-F116H can encapsulate three rFasx molecules (36 kDa, total, loading ratio of 60:15) (AUC peaks are labelled with the number of encapsulated POI with colors corresponding to the molar ratios of titrated POI during the folding protocol.). **b**, tES-F116H charge is a critical determinant of encapsulation efficiency. Positively charged rFasx exhibits no encapsulation in tES-F116H(+). **c**, two rLuc molecules (72 kDa, total, loading ratio of 60:10) can be accommodated in tES-F116H. **d**, negatively charged rLuc shows optimal encapsulation in tES-F116H(+). **e**, tES accomodates one HSA (66 kDa, total, loading ratio of 60:5) molecule. **f**, negatively charged HSA shows optimal encapsulation in tES-F116H(+).

Figure 3

Monomeric POI encapsulation using tES-F116H a, tES-F116H can encapsulate three rFasx molecules (36 kDa, total, loading ratio of 60:15) (AUC peaks are labelled with the number of encapsulated POI with colors corresponding to the molar ratios of titrated POI during the folding protocol.). b, tES-F116H charge is a critical determinant of encapsulation efficiency. Positively charged rFasx exhibits no encapsulation in tES-F116H(+). c, two rLuc molecules (72 kDa, total, loading ratio of 60:10) can be accommodated in tES-

F116H. d, negatively charged rLuc shows optimal encapsulation in tES-F116H(+). e, tES accomodates one HSA (66 kDa, total, loading ratio of 60:5) molecule. f, negatively charged HSA shows optimal encapsulation in tES-F116H(+).

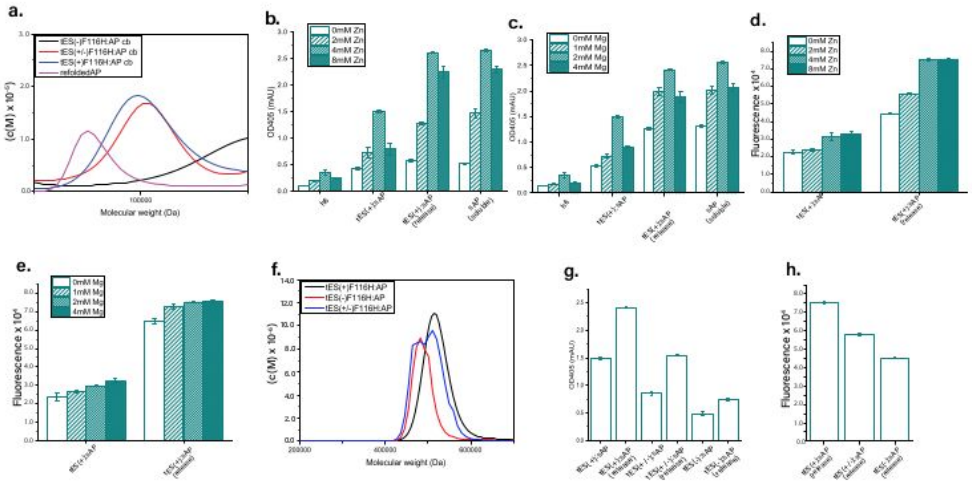

Fig. 4 | Alkaline phosphatase folding with tES-F116H. a, Release of sAP from tES-F116H charge variants results in a dimeric peak for tES-F116H(+) and tES-F116H(+/-), however monomeric sAP was observed with sAP folded alone and aggregation was seen with the use of tES-F116H(-).**b**, **c**, Titration of Zn and Mg yields activity increases similar for caged versus released sAP and a solubly expressed sAP control.**d, e**, Titration of Zn and Mg have differential effects on sAP intrinsic fluorescence, a marker of folding. **f**, AUC of tES-F116H(+) loaded with sAP demonstrates a M.W. of 522 kDa, consistent with encapsulation of a single sAP monomer. **g**, Activity of sAP is moderately increased after release from three charge varients of tES-F116H. **h.** Intrinsic fluorescence is optimal when sAP is folded with charge-matched tES-F116H(+).

Figure 4

Alkaline phosphatase folding with tES-F116H. a, Release of sAP from tES-F116H charge variants results in a dimeric peak for tES-F116H(+) and tES-F116H(+/-), however monomeric sAP was observed with sAP

folded alone and aggregation was seen with the use of tES-F116H(-).b, c, Titration of Zn and Mg yields activity increases similar for caged versus released sAP and a solubly expressed sAP control.d, e, Titration of Zn and Mg have differential effects on sAP intrinsic fluorescence, a marker of folding. f, AUC of tES-F116H(+) loaded with sAP demonstrates a M.W. of 522 kDa, consistent with encapsulation of a single sAP monomer. g, Activity of sAP is moderately increased after release from three charge varients of tES-F116H. h. Intrinsic fluorescence is optimal when sAP is folded with charge-matched tES-F116H(+).

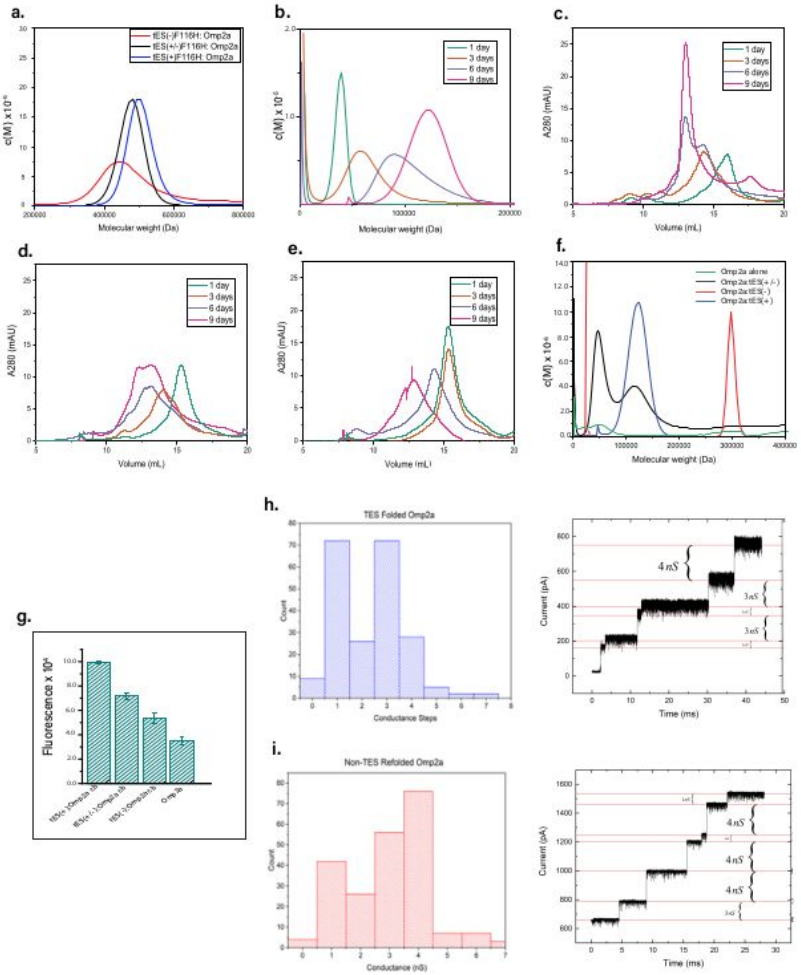

Fig. 5 | Omp2a folding with tES-F116H. **a**, tES-F116H(+) encapsulates a single monomer of Omp2a **b**, Omp2a monomers released from tES-F116H(+) form trimeric assembiles after a 9 day incupation period. **c**,**d**,**e**, SEC demonstrates complete trimerization only in the setting of tES116H(+) mediated folding. **f**, AUC demonstrates the ability to form Omp2a trimers is effected by tES-F116H internal charge. Omp2a folded without tES-F116H does not demonstrate trimerization. **g**, Intrinsic fluorescence of Omp2a refolded and released from tES(+)F116H, tES(+/-)F116H and tES(-)F116H ,and Omp2a refolded without tES. **h**, Conductance measurements of the 172 kDa Omp2a trimeric SEC fraction demonstrate a range of 1 nS to 4 nS. **i**, A positive control of Omp2a demonstrates similar conductance insertions.

Figure 5

Omp2a folding with tES-F116H. a, tES-F116H(+) encapsulates a single monomer of Omp2a b, Omp2a monomers released from tES-F116H(+) form trimeric assembiles after a 9 day incupation period. c,d,e, SEC demonstrates complete trimerization only in the setting of tES116H(+) mediated folding. f, AUC demonstrates the ability to form Omp2a trimers is effected by tES-F116H internal charge. Omp2a folded without tES-F116H does not demonstrate trimerization. g, Intrinsic fluorescence of Omp2a refolded and released from tES(+)F116H, tES(+/-)F116H and tES(-)F116H ,and Omp2a refolded without tES. h, Conductance measurements of the 172 kDa Omp2a trimeric SEC fraction demonstrate a range of 1 nS to 4 nS. i, A positive control of Omp2a demonstrates similar conductance insertions.

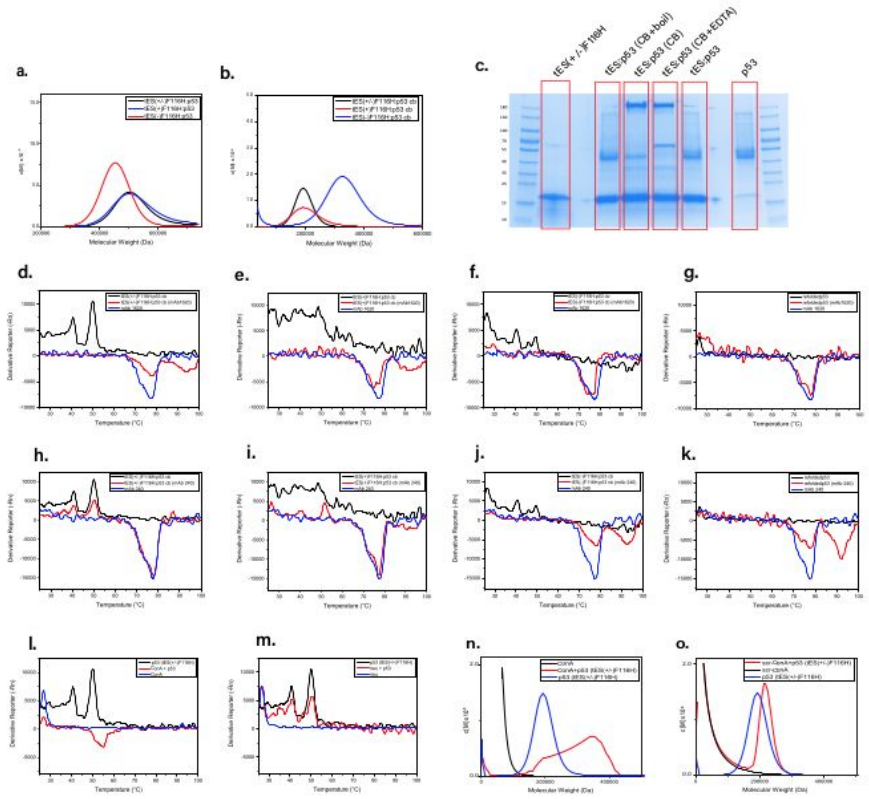

Fig. 6 | p53 folding and tetramerization using tES-F116H. **a**, AUC demonstrates tES-F116H(+/-) and tES-F116H(+) encapsulatd a single p53 monomer. **b**, p53 replease from tES-F116H(+/-) and tES-F116H(+) results in tetramer formation as demonstrated by AUC. The use of tES-F116H(-) results in aggregation. **c,** SDS gel demonstrates monomeric p53 in the tES:POI complex, and tetrameric p53 after monomer release. Boiling of tetrameric sample (lane 4) results in p53 monomers (lane 3). Differential scanning fluorimetry of mAb1640, p53 and a 1:1 mixure **d**, tES-F116H(+/-) **e**, tES-F116H(+) **f**, tES-F116H(-) **g**, p53 folded without tES. p53 folded with tES-F116H(+/-) shows a characteristic tetramer denaturation peak at 50 °C. Addition of mAb1620 results in a novel complex peak at ~95°C. Differential scanning fluorimetry of mAb240, p53 and **h**, tES-F116H(+/-) **i**, tES-F116H(+) **j**, tES-F116H(-) **k**, p53 folded without tES. p53 denaturation is affected by conA (**l**) but not a scrambled sequence (**m**). AUC analysis of tES-F116H(+/-) folded tetramers demonstrates complex formation in the presence of ConA (**n**) but not in the presence of scr-conA (**o**).

Figure 6

p53 folding and tetramerization using tES-F116H. a, AUC demonstrates tES-F116H(+/-) and tES-F116H(+) encapsulatd a single p53 monomer. b, p53 replease from tES-F116H(+/-) and tES-F116H(+) results in tetramer formation as demonstrated by AUC. The use of tES-F116H(-) results in aggregation. c, SDS gel demonstrates monomeric p53 in the tES:POI complex, and tetrameric p53 after monomer release. Boiling of tetrameric sample (lane 4) results in p53 monomers (lane 3). Differential scanning fluorimetry of

mAb1640, p53 and a 1:1 mixure d, tES-F116H(+/-) e, tES-F116H(+) f, tES-F116H(-) g, p53 folded without tES. p53 folded with tES-F116H(+/-) shows a characteristic tetramer denaturation peak at 50 oC. Addition of mAb1620 results in a novel complex peak at ~95oC. Differential scanning fluorimetry of mAb240, p53 and h, tES-F116H(+/-) i, tES-F116H(+) j, tES-F116H(-) k, p53 folded without tES. p53 denaturation is affected by conA (l) but not a scrambled sequence (m). AUC analysis of tES-F116H(+/-) folded tetramers demonstrates complex formation in the presence of ConA (n) but not in the presence of scr-conA (o).

Supplementary Files

This is a list of supplementary files associated with this preprint. Click to download.

- Supplementary.pdf
- Supplementary.pdf